AIP | Review of Scientific Instruments

Optimized instrumentation for edge Te and ne measurements on COMPASS-D tokamak from HeI line intensity ratios

A. R. Field, P. G. Carolan, N. J. Conway, and M. G. O'Mullane

Citation: Rev. Sci. Instrum. **70**, 355 (1999); doi: 10.1063/1.1149504
View online: http://dx.doi.org/10.1063/1.1149504
View Table of Contents: http://rsi.aip.org/resource/1/RSINAK/v70/i1
Published by the American Institute of Physics.

Related Articles

Spherical torus equilibria reconstructed by a two-fluid, low-collisionality model
Phys. Plasmas 19, 102512 (2012)

Oblique electron-cyclotron-emission radial and phase detector of rotating magnetic islands applied to alignment and modulation of electron-cyclotron-current-drive for neoclassical tearing mode stabilization
Rev. Sci. Instrum. 83, 103507 (2012)

Toroidal rotation of multiple species of ions in tokamak plasma driven by lower-hybrid-waves
Phys. Plasmas 19, 102505 (2012)

Perpendicular dynamics of runaway electrons in tokamak plasmas
Phys. Plasmas 19, 102504 (2012)

Electron cyclotron current drive modelling with parallel momentum correction for tokamaks and stellarators
Phys. Plasmas 19, 102501 (2012)

Additional information on Rev. Sci. Instrum.

Journal Homepage: http://rsi.aip.org
Journal Information: http://rsi.aip.org/about/about_the_journal
Top downloads: http://rsi.aip.org/features/most_downloaded
Information for Authors: http://rsi.aip.org/authors

ADVERTISEMENT

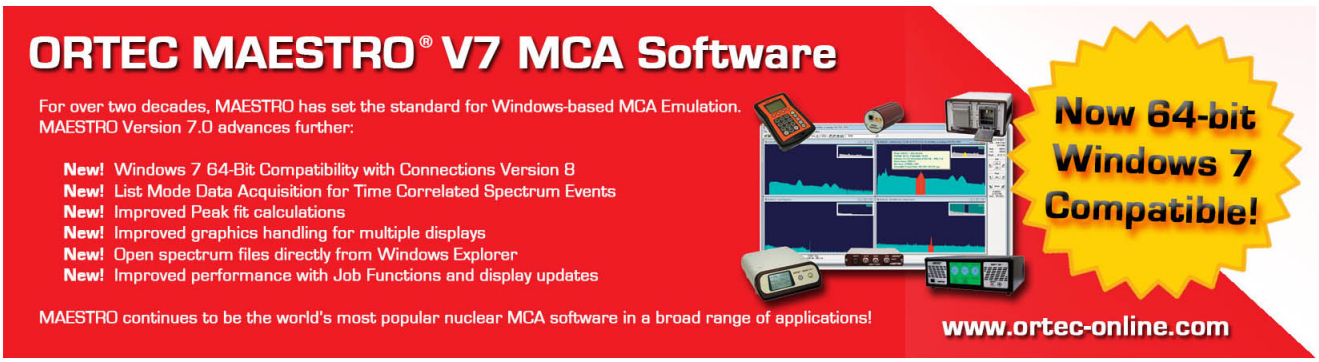

Optimized instrumentation for edge T_e and n_e measurements on COMPASS-D tokamak from He I line intensity ratios

A. R. Field and P. G. Carolan
Euratom/UKAEA Fusion Association, Culham Science Centre, Abingdon, Oxon OX14 3DB, United Kingdom

N. J. Conway
University College Dublin, Republic of Ireland

M. G. O'Mullane
Department of Physics and Applied Physics, University of Strathclyde, Glasgow G4 0NG, United Kingdom

(Presented on 8 June 1998)

Instrumentation has been developed for the measurement of electron temperature and density profiles at the boundary of COMPASS-D tokamak plasmas from He I line intensities. The technique is applicable to measurements of n_e and T_e over the relevant ranges of $10^{17}-10^{20}$ m^{-3} and 10–500 eV. Spectra from eight viewing chords viewing a thermal helium jet are recorded on a CCD sensor with ≈1 ms time resolution. A 0.6 m Czerny-Turner spectrometer, corrected for astigmatism using an internal, cylindrical lens optimizes throughput by availing of a 110×110 mm^2, 300 l/mm grating. n_e and T_e profile measurements from L-mode (low) and quiescent H-mode (high) confinement plasmas are presented. [S0034-6748(99)54310-4]

I. INTRODUCTION

Detailed knowledge of the behavior of the electron temperature T_e and density n_e profiles at the boundary of tokamak plasmas is required for studies of plasma confinement and exhaust. In particular, measurements of the steep edge gradients which develop during regimes of improved confinement (H-mode) require good spatial (≈5 mm) and temporal (≈1 ms) resolution. The determination of edge T_e and n_e profiles from the ratios of atomic line intensities offers measurements which are relatively nonperturbative compared with those from Langmuir probes.

Line emission from atomic helium puffed at the plasma boundary can provide localized measurements and this method has been utilized on several devices.[1–3] Atomic helium is well suited for this measurement owing to its relatively high ionization energy (24.6 eV) which allows thermal helium to penetrate the edge plasma. There exist singlet-singlet (668/728 nm) and singlet-triplet (728/706 nm) line ratios which are mainly sensitive to n_e and T_e, respectively. Conveniently, these three lines are closely grouped in wavelength.

A dedicated multichord spectrometer system has been developed for such measurements on the COMPASS-D tokamak.[4] For a given spectral resolution, the grating size and ruling density determines the light collection efficiency and for this reason we use a relatively large spectrometer. Measurements are localized by viewing orthogonally to a thermal helium jet.

Results from ECRH (electron cyclotron resonance heating) heated plasmas exhibiting L- (low) and H-mode (high) confinement regimes are presented.

II. ATOMIC DATA

Measurement of T_e from He I line intensity ratios was first proposed by Cunningham.[5] Excitation rates of singlet and triplet levels with the same principle quantum number n have quite different T_e dependencies because the spin-exchange excitation of the triplet levels from the $1\,^1S$ ground state involves resonant electron exchange.[6] Thus for temperatures above the excitation energy of the triplet level ΔE_{kl} the relative triplet/singlet excitation rates decrease with T_e.

Because of the two metastable levels $2s\,^1S$ (20.6 eV) and $2s\,^3S$ (19.8 eV) the population distribution departs from a coronal distribution, which neglects collisional deexcitation, at relatively low densities ($>10^{17}$ m^{-3}) and, thus, requires a full collisional radiative (CR) treatment. As a consequence, the populations of different l levels (orbital quantum number) of equal n within the singlet (or triplet) systems are density dependent and this allows for measurement of n_e from suitable line ratios. Details of such CR calculations are given elsewhere.[6–8] Recommended line pairs from the $n=3$ level are 667.8/728.1 nm ($3d\,^1D$-$2p\,^1P$/$3s\,^1S$-$2p\,^1P$) for the n_e measurement and 728.1/706.5 nm ($3s\,^1S$-$2p\,^1P$/$3s\,^3S$-$2p\,^3P$) for the T_e measurement. These lines have been used successfully elsewhere.[1–3] Other transitions from the $n=4$ levels (471.3, 492.2, 501.6, 504.8 nm) are discussed[9] but generally are not sufficiently intense to be used in practice and excitation of the 501.6 nm line (from $4s\,^1S$) by resonant photon absorption from the ground state also complicates the interpretation.

In this work we use effective excitation rates obtained from the atomic data analysis system (ADAS),[10] which computes a full CR model for the 19 levels with $n\leqslant4$. Figure 1 shows the intensity ratios $R_1=I$(667.8 nm)/I(728.1 nm) and $R_2=I$(728.1 nm)/I(706.5 nm) as functions of n_e and T_e, respectively.

Inversion of measured ratios R_{1m} and R_{2m} in terms of n_e and T_e is performed using the following procedure: the $R_{1,2}$

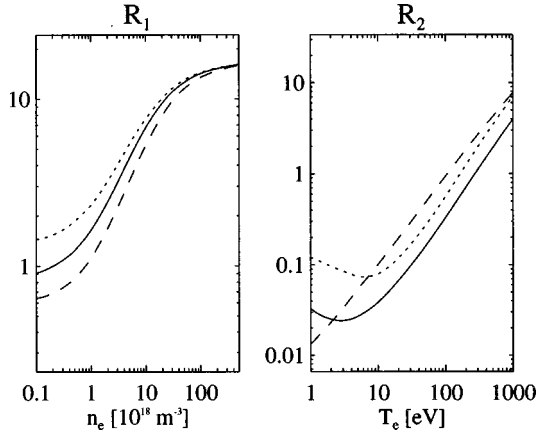

FIG. 1. Intensity ratios $R_1(n_e)$ and $R_2(T_e)$ obtained from ratios of effective excitation coefficients (Ref. 10). Data corresponding to various values of T_e (30, 100 and 300 eV) and n_e (10^{18}, 10^{19} and 10^{20} m^{-3}) are shown as dotted, solid and dashed lines, respectively.

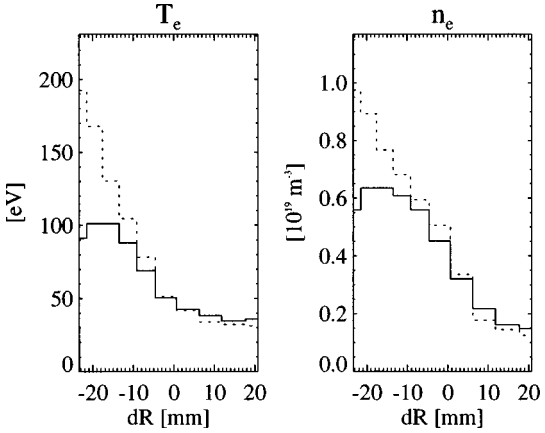

FIG. 2. Comparison of local values of T_e and n_e (dashed lines) with values determined from ratios $R_{1,2}$ of simulated line-integral intensities (solid lines) for a ratio of recycling to injected He flux densities of 1%. Radial positions dR are relative to a nominal separatrix location.

data, available at discrete values $(n_{e,i}, T_{e,j})$, are fitted with splines and these are used to find a set of $n_e(T_{e,j})$ and $T_e(n_{e,i})$ which satisfy the measured ratios; these values are splined again and, being approximately orthogonal in (n_e, T_e), the resulting curves intersect at a location $(n_{e,m}, T_{e,m})$ which satisfies both measured ratios.

At low values of R_2 this process does not always yield a unique solution. This is because, at low values of n_e, R_2 does not increase monotonically with T_e. We select the higher T_e branch only, the lower being well below ($T_e < 7$ eV) the values typical for the boundary plasma.

III. SPATIAL RANGE AND RESOLUTION

Ionization loss reduces the emission from the thermal helium as it penetrates the edge plasma. The measurement is therefore limited in range to a line-density of order $n_e\lambda_i$ (where λ_i is the ionization length) which is typically 10^{17} m^{-2} at 50 eV for 300 K thermal atoms. Atoms with velocities appreciably greater than the mean thermal speed ν_{th} will penetrate further into the plasma. The accuracy with which the weak emission from these can be measured determines the spatial range of the measurement. A collimated helium beam, together with well focused collection optics and low levels of background helium are required to optimize the range.

For simplicity, we puff helium from a tube located at the vessel wall 3 cm above the midplane. The gas plume diverges from the tube at a full-cone angle of $\approx 40°$ resulting in a ≈ 4 cm poloidal spread at the plasma. By viewing the plume directly from above smearing due to spatial averaging along the lines of sight can be minimized. Simulations show that this results in only small differences ($\approx 3\%$) between actual values of T_e and n_e and those determined from ratios of line-integral intensities within a region extending ± 2 cm of either side of the separatrix (edge of confined plasma).

A more serious problem is the ''halo'' of emission from the helium puffed during the discharge, which is not pumped and thus recycles from the walls. At the end of the discharge, when, typically, 10^{18} He atoms have been injected, the flux density of the halo is $\approx 1\%$ of that at the nozzle. Simulations show that, for the innermost chords, the line-integrated ''halo'' emission dominates the weaker emission directly from the jet. As shown in Fig. 2, this causes the measured line-averaged values of T_e and n_e to underestimate the actual local values substantially at locations more than ≈ 1 cm inside the separatrix.

As well as being limited by the collection optics, the spatial resolution is limited by the time τ_r taken for the atomic level populations to adjust to local conditions. From a CR model Schweer[1] has determined the time required for the slowest level to equilibrate. This is approximately constant with T_e and proportional to n_e^{-1}. For thermal gas the spatial resolution can be parametrized in terms of $\lambda_r = \tau_r \nu_{\text{th}}$ and $n_e\lambda_r \approx 5\times 10^{15}$ m^{-2} for gas at 300 K, so a resolution of 5 mm is achievable at a density of 10^{18} m^{-3}.

IV. INSTRUMENTATION

Helium is injected through a 4 mm tube 3 cm above the midplane at the vessel wall, 5 cm from the separatrix. As shown in Fig. 3, the gas plume is observed from above from a vertical port at $R_m = 0.693$ m. An array of eight 400-μm-diam quartz fibers[11] at 1.7 mm pitch is imaged at the plane of the nozzle using a 100 mm, F/2 camera lens mounted above the window. This results in a chord spacing of 5.2 mm, covering 36 mm, and a resolution of ≈ 2 mm at the nozzle. The lens is mounted in a goniometer to facilitate alignment.

The helium flux is regulated by pulsing a piezoelectric valve allowing $\approx 10^{18}$ atoms into an intermediate volume. The low conductance of the 4 mm tube results in a more steady influx of $\approx 10^{19}$ s^{-1} into the vessel ($\tau_{\text{rise}}/\tau_{\text{decay}} = 30/100$ ms).

When selecting an appropriate spectrometer we took note that for a given resolution $d\lambda$ the throughput is directly proportional to the grating size rather than, as often thought, the f-number of the spectrometer. The light throughput at the output I_{op} is given by

$$I_{\text{op}} \cong I(\lambda)\, d\lambda^2 \epsilon N H (h/f) = I(\lambda)\, d\lambda^2 \epsilon A g (h/f), \qquad (1)$$

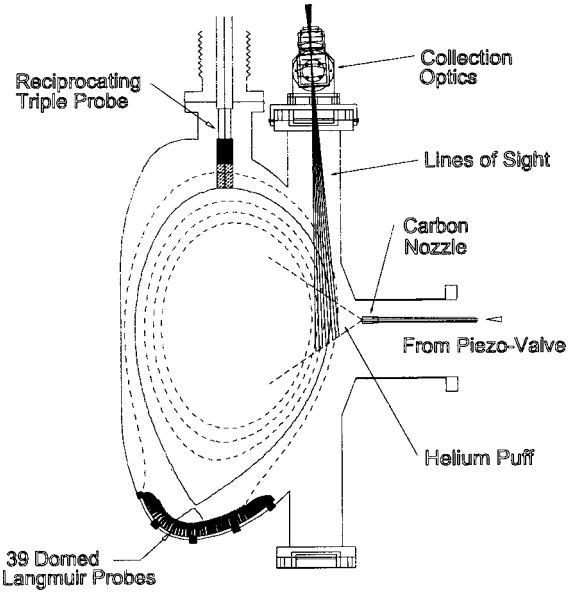

FIG. 3. A poloidal cross section of the COMPASS-D vacuum vessel showing the location of the helium gas puff, the HELIOS collection optics and the Langmuir probe diagnostics (reciprocating and divertor array).

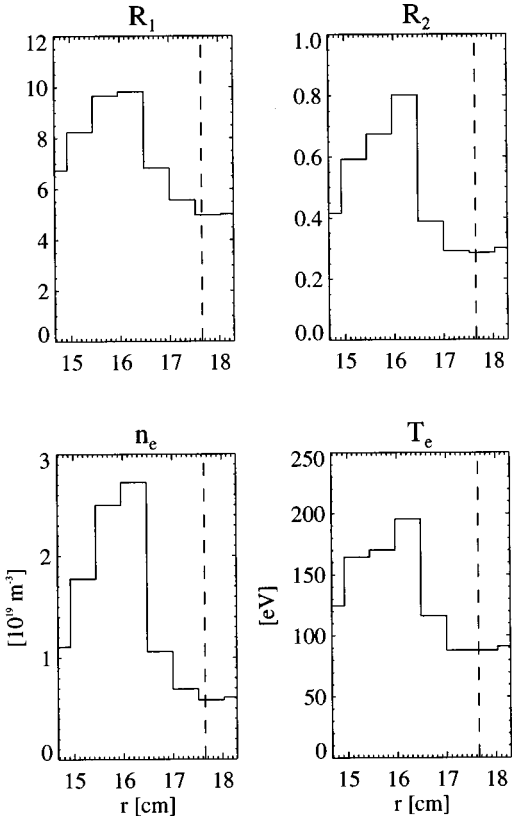

FIG. 4. Measured He I intensity ratios $R_{1,2}$ from the eight viewing chords and the radial profiles of n_e and T_e determined from these ratios for discharge #26674 at 0.17 s during the H-mode phase. The expected location of the separatrix is indicated (minor radii r are relative to a major radius of 0.557 m).

where N is the number of rulings, g the ruling density, ϵ the efficiency, H the height and A the area of the grating, f is the focal length of the spectrometer and h the input slit height.

The ''HELIOS'' (helium optical spectrometer) system uses a 0.6 m Czerny-Turner spectrometer (Rank-Hilger M600) with a 110×110 mm^2 grating. The fiber array, here of 0.84 mm pitch, is imaged at the entrance slit using a conjugate pair of 35 mm cameral lenses (100 mm, F/2:50 mm, F/1.2) which match the aperture of the fibers (0.23 N.A.) to that of the spectrometer (F/4.5). A similar pair of lenses is used to image the exit focal plane at the CCD sensor.

Inherent astigmatism of the Czerny-Turner configuration is overcome by moving the sagittal focal plane so that it coincides with the tangential focus using an $f=300$ mm cylindrical lens between the collimating mirror and the exit plane. The optimal radial focus found by ray tracing has an rms extent of 65 μm. The measured cross talk between adjacent chords is $<1\%$ of the peak intensity.

With a 300 l mm^{-1} grating the inverse dispersion at the CCD is 10.94 nm/mm (including 2:1 reduction lenses). This results in a spectral coverage over the 365 active columns of the sensor of 88 nm, which encompasses the three He I lines.

The CCD system (Wright Instruments Ltd., No. P059, Enhanced II Electronics) incorporates an EEV (English electric valve) back-illuminated sensor (CCD02-06-2-232) with 385×578 22 μm^2 pixels and a peak quantum efficiency of 60% at 650 nm.[12] This is Peltier cooled to 200 K resulting in typical dark current of 0.6 e/s/pixel. Accumulated charge can be shifted independently in the image and store regions at 1 μs vertical row transfer time. The charge accumulated in the group of rows corresponding to a chord (≈30) can thus be ''binned'' into a single row in the store region. In total 36 frames of eight chords can be stored per discharge.

The camera has a 16-bit, dual speed analog-to-digital converter (ADC) with 5.2 or 34 μs digitization time. An interface card provides for control from a PC where a Windows© based software driver allows for definition of arbitrary binned regions and timing sequences. External triggers and a clock output allow for synchronization with the discharge and other measurements. The store region is read out after the discharge with typically 5.6 e rms readout noise. A preamplifier matches the full-well capacity of the sensor (3.7×10^5 e) to the range of the ADC, resulting in 20 e/count for 15-bit data (1-bit right shifted).

Binning of the eight chords requires a time $\tau_{\rm bin}$ which is the sum of vertical transfer times for the image and store regions τ_ν (1 μs) and the mode switch times τ_m (2 μs):

$$\tau_{\rm bin}=\sum_{j=1}^{N}\left[(n_j+1)\tau_\nu+2\tau_m\right]. \tag{2}$$

If the chords occupy the whole image region this amounts to 322 μs. Measurements are typically made with a frame rate $\tau_{\rm fr}$ of 2 ms.

As the fibers are aligned vertically at the sensor, during the binning period, some light from chords closer to the store region ($j<i$) will contribute to the signal S_i measured in a particular chord i. There will also be a contribution from chords farther from the store region ($j>i$) remaining from the prior binning period. This temporal ''smearing'' of order $\tau_{\rm bin}/\tau_{\rm fr}$ (typically 16% for uniform illumination) is corrected at the analysis stage for each column of the sensor. If it is

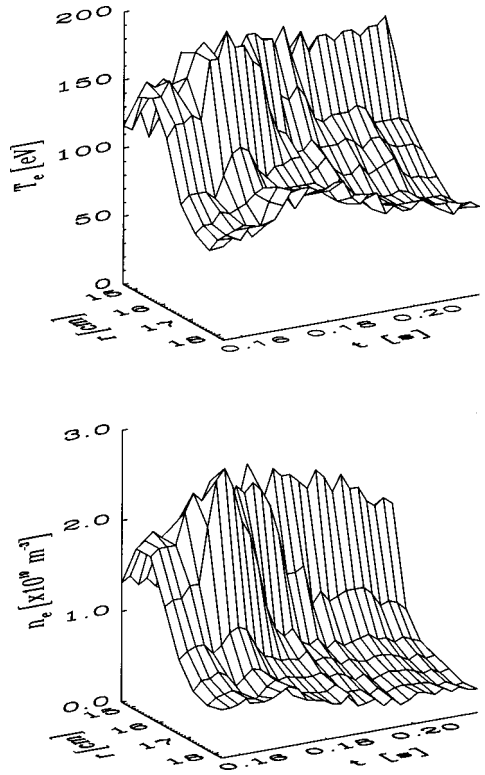

FIG. 5. The temporal evolution of measured T_e and n_e profiles during a discharge exhibiting L- and H-mode confinement with the L/H-transition at 0.163 ms (#26674 with $B_t=-2.1$ T, $I_p=160$ kA, $\overline{n_e}=5\times10^{19}$ m^{-3}).

assumed that the incident intensities I_i change slowly in time, these can be determined from the measured signals S_i by solving the linear system:

$$S_i=a_{ij}I_j, \tag{3}$$

where the matrix elements a_{ij} represent the proportional contribution of light from each chord j to the intensity measured in chord i in terms of the row count n_i and row transfer and mode switch times:

$$\begin{aligned} a_{ij}&=(n_j+1)\tau_v+2\tau_m, \quad i\neq j,\\ a_{jj}&=(n_j+1)\tau_v+\tau_{\mathrm{fr}}-\tau_{\mathrm{bin}}. \end{aligned} \tag{4}$$

The typical frame-to-frame change in the intensity of $<10\%$ ensures that the above approximation results in small errors of $<5\%$ in the correction, which is itself of order 20% resulting in overall errors of $<1\%$.

V. RESULTS

In a typical spectrum measured with a helium influx of $\approx10^{19}$ s^{-1} into a deuterium discharge with ECRH heating and a line-average density of 5×10^{19} m^{-3}, the He I lines are well separated from any intrinsic impurity lines, the carbon II lines at 678 and 712 nm being the strongest present. The strongest He I (667.8 nm) line exhibits peak count rates of typically 5×10^6 ct/s/pixel. Minimum signals for the weakest He I line are $\approx$200 counts in 2 ms equivalent to $\leqslant4\%$ statistical error.

Figure 4 shows radial profiles of the ratios $R_{1,2}$ of the 667.8/728.1 and 728.1/706.7 nm lines measured during the H-mode phase of discharge #26674 at 0.17 s. Corresponding values of n_e and T_e determined from these ratios are also shown. The plasma, which is heated by 700 kW of ohmic and ECRH power, exhibits a transition from L- to H-mode at 0.163 s. Gradients in n_e and T_e increase sharply during the H-mode ≈1 cm inside the separatrix, the location of which is determined from equilibrium reconstruction[13] and has an estimated uncertainty of ±5 mm. Maximum measured values of T_e and n_e of 200 eV and 2.7×10^{19} m^{-3} correspond to an electron pressure gradient approaching 150 kPm^{-1}. Further into the plasma the measured values decrease, underestimating the actual local values because of the spatial smearing effects discussed above. The temporal development of T_e and n_e is shown in Fig. 5. It can be seen that, later in the quiescent H-mode phase, these gradients decrease and there is an inward shift of the profiles.

The observed change in sign of the gradients at smaller radii (chords 6-8) is due to the instrumental effects discussed earlier, principally spatial smearing, causing the measured values to underestimate actual local values (see also Figs. 2 and 4). The measurements from HELIOS in the region outside the separatrix have been shown to be consistent with edge Langmuir probe measurements from similar conditions during earlier campaigns. Improvements to the system are planned, including provision of a well collimated, supersonic thermal helium jet[6] which should help overcome the limitations described above and extend the spatial range of reliable measurements.

ACKNOWLEDGMENT

This work was jointly funded by the U.K. Department of Trade and Industry and Euratom.

[1] B. Schweer, G. Mank, A. Pospieszczyk, B. Brosda, and B. Pohlmeyer, J. Nucl. Mater. **196–198**, 174 (1992).
[2] S. J. Davies *et al.*, J. Nucl. Mater. **241–243**, 426 (1997).
[3] H. Behrendt *et al.*, in *Proceedings of the 21st EPS Conference on Controlled Fusion and Plasma Physics, Montpellier, France, 1994, Vol III* (EPS, Geneva, 1994), p. 1328.
[4] S. J. Fielding, M. Valovic, P. G. Carolan, D. A. Gates, C. Hunt, P. Leahy, A. W. Morris, and the COMPASS-D Physics and ECRH Teams, Plasma Phys. Controlled Fusion **40**, 731 (1998).
[5] S. P. Cunningham, Conference on Thermonuclear Reactors, U.S. Atomic Energy Commission Report No. 279, Livermore, 1955, p. 289.
[6] P. Kornejew, PH.D. thesis, Humboldt-Universität, Berlin, 1996, IPP Report, IPP-8/10, 1996.
[7] B. Brosda, Ph.D. thesis, Rühr Universität, Bochum, 1993.
[8] S. Sasaki, S. Takamura, and T. Kato, Fusion Eng. Des. **34–35**, 747 (1997).
[9] S. Sasaki, S. Takamura, S. Watanabe, S. Masuzaki, T. Kato, and K. Kadota, Rev. Sci. Instrum. **67**, 3521 (1996).
[10] H. P. Summers, ''Atomic data and analysis structure,'' JET Report, JET-IR (94) 06.
[11] CeramOptec, GmbH, Germany.
[12] Wright Instruments Ltd., Unit 10, 26 Queensway, Enfield, Middlesex, EN3 4SA, UK.
[13] L. L. Lao, J. R. Ferron, R. J. Groebner, W. Howl, H. St. John, E. J. Strait, and T. S. Taylor, Nucl. Fusion **30**, 1035 (1990).